Unlocking the Aromatic Cope Rearrangement with Gold(I) Catalysis

Pierre Locquet, Akilan Rajamani, Rémi Pereira, Fabienne Grellepois, Jean-Marc Weibel, Eric Hénon, Emmanuel Riguet, Aurélien Blanc

▶ **To cite this version:**

Pierre Locquet, Akilan Rajamani, Rémi Pereira, Fabienne Grellepois, Jean-Marc Weibel, et al.. Unlocking the Aromatic Cope Rearrangement with Gold(I) Catalysis. ACS Catalysis, 2024, 14 (24), pp.18884. ⟨10.1021/acscatal.4c06662⟩. ⟨hal-04764412v2⟩

HAL Id: hal-04764412

https://hal.science/hal-04764412v2

Submitted on 7 Jul 2025

HAL is a multi-disciplinary open access archive for the deposit and dissemination of scientific research documents, whether they are published or not. The documents may come from teaching and research institutions in France or abroad, or from public or private research centers.

L'archive ouverte pluridisciplinaire **HAL**, est destinée au dépôt et à la diffusion de documents scientifiques de niveau recherche, publiés ou non, émanant des établissements d'enseignement et de recherche français ou étrangers, des laboratoires publics ou privés.

HAL Authorization

Unlocking the Aromatic Cope Rearrangement with Gold(I) Catalysis

Pierre Locquet,[a‡] Akilan Rajamani,[b‡] Rémi Pereira,[b] Fabienne Grellepois,[b] Jean-Marc Weibel,[a] Eric Hénon,*[,b] Emmanuel Riguet*[,b] and Aurélien Blanc*[,a]

[a]Université de Strasbourg, CNRS, Institut de Chimie, UMR 7177, 4 rue Blaise Pascal, CS 90032, 67081 Strasbourg, France.

[b]Université de Reims Champagne-Ardenne, CNRS, Institut de Chimie Moléculaire de Reims, UMR 7312, 51097 Reims, France.

ABSTRACT: The Aromatic Cope Rearrangement (ArCopeR) is a highly challenging chemical reaction under thermal conditions, primarily attributed to the loss of aromaticity during the initial [3,3]-sigmatropic step of the process. Such rare transformation typically requires high temperatures and specially engineered 1,5-hexadiene scaffolds, making it impractical for straightforward synthesis of new molecules. Here, we demonstrated that gold(I) catalysts significantly lower the energetic barriers associated to ArCopeR, enabling the reaction to be carried out at low temperature (rt to 70°C) in dichloroethane or hexafluoroisopropanol with high yields. Specifically, phosphine gold(I) complex ((*p*-CF_3Ph)$_3$PAuOTf) permits for the diastereoselective and divergent aromatic Cope rearrangement from various α-allyl-α'-heteroaromatic γ-lactone or malonate derivatives, while N-heterocyclic carbene gold(I) (IPrAuNTf_2) allows the selective dearomatization reaction. Extended quantum mechanics calculations, consistent with experimental observations, reveal that (i) an interweaved transformation occurs instead of the expected ArCope cascade made of formal [3,3]-sigmatropic rearrangement and [1,3]H-shift steps, and that (ii) van der Waals interactions between the catalyst and substrate contribute to the interrupted ArCope process leading to dearomatize products. This study presents the first catalytic and synthetically useful protocol to promote ArCopeR under mild conditions.

1. INTRODUCTION

In the early forties, Arthur C. Cope *et al.* reported the concerted rearrangement of 1,5-hexadienes and of derivatives under thermal conditions.[1] Named after this seminal work, the Cope rearrangement has since become a classic and fruitful synthetic method, often used as key step in the synthesis of many natural and bioactive products.[2] Nevertheless, Arthur C. Cope failed to achieve the rearrangement of one kind of 1,5-hexadiene scaffolds, those in which one double bond is embedded within an aromatic ring.[3] Nearly seven decades later, such so-called Aromatic Cope Rearrangements (ArCopeR) are still a challenge as reflected by the rare publications on this transformation, around forty including aromatic oxy-Cope reaction.[4] Actually, the ArCopeR are entangled by drastic energetic problems severely limiting its development (**A** in Scheme 1). Its first step, a [3,3]-sigmatropic rearrangement, requires a loss of aromaticity and thus implies high thermodynamic and kinetic impediments.[5] The second step, a [1,3]H-shift, is symmetrically or geometrically forbidden in a concerted reaction.[6] Both difficult steps clearly upset the synthetic utility of this rearrangement typically requiring high temperature to be performed (>100°C).

Only a few thermal approaches based on the rationally designed substrates to circumvent this challenging transformation have been reported including cyclopropane/butane strain-released,[4,7] appropriate aromatic and 1,5-hexadiene scaffolds,[8] or synchronized aromaticity strategy[9] (**B** in Scheme 1). Nonetheless, the expected products could be structurally highly valuable as the reaction permit the regio- and stereospecific C-H functionalization of aromatic rings and, if the ArCopeR is stopped after the [3,3]-sigmatropic rearrangement (Interrupted ArCopeR, **A** in Scheme 1), dearomatization occurs leading to tridimensional complex molecules. In this field, MacDowell *et al.*[10] reported in 1993 that 1,5-hexadiene derivatives not embedded in polycyclic scaffold such as α-allyl-α'-aryl or heteroaryl malonate derivatives (**B**, left box in Scheme 1) afforded the ArCope products under harsh conditions (≥180°C) with moderate yields, along with sometimes abnormal[11] ArCope side-products. Based on this precedent, we have already demonstrated that the incorporation of a lactone motif in place of malonate facilitates the [3,3]-sigmatropic step enabling the ArCopeR to be thermally performed at 165°C in higher yields in the presence of Et_3N to favor the [1,3]H-shift step.[12] Nevertheless, the harsh thermal conditions employed still limit the reaction to be synthetically useful. There is thus a strong need to decrease the activation barrier of the [3,3]-sigmatropic process.

In few cases, external transition metals have proved to be effective to alter the potential energy surface and decrease the activation barrier of pericyclic reactions through 'transition-state complexation'.[13] In line with such strategy, Gagné *et al.*[14] reported that the asymmetric Cope rearrangement of specific vinylcyclopropane derivatives was efficiently catalyzed by a chiral xylyl-BINAP digold(I) complex. Therefore, we were wondering whether gold catalysis[15] could solve issues related to the ArCopeR energetic requirements. Supported by calculations, we report herein that gold(I)-based catalysts can strongly lower the energy barriers of the ArCopeR and thus to perform diastereoselective and divergent aromatic Cope rearrangement or selective

dearomatization reaction under mild reaction conditions (rt to 70°C) and high yields (**C** in Scheme 1).

Scheme 1. (**A**) Impediments of the Aromatic Cope Rearrangement, (**B**) Thermal ArCopeR Strategies and (**C**) Gold(I)-Catalyzed ArCopeR.

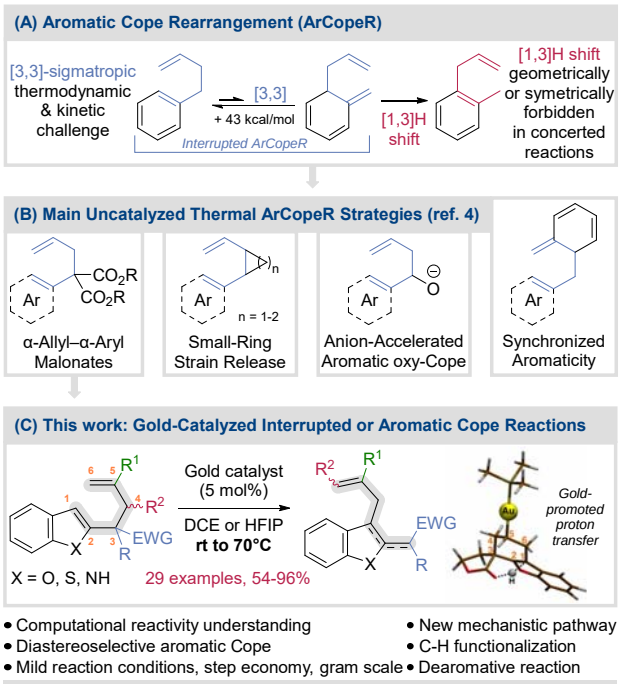

2. RESULTS AND DISCUSSION

2.1. Preliminary Computational Exploration of Gold(I)-Catalyzed ArCope.

Prior to experimental study, theoretical calculations were conducted to investigate the ArCope mechanism alteration induced by the presence of cationic gold(I) complexes on α-allyl-α'-benzofuran γ-lactone derivatives **1**. Considering the carbophilic Lewis acidity of gold(I) allowing metal interaction with the double bonds, the [3,3]-sigmatropic rearrangement is the most susceptible step affected during this transformation. In our previous study,[12b] we showed by DFT calculations that for the uncatalyzed system the [3,3]-sigmatropic rearrangement proceeds through a single transition state (TS) involving a relatively large energy barrier for **1a** (R^1, R^2=H) at 40°C (40.0 kcal.mol^{-1}). This TS is associated with the C3–C4 bond rupture together with the simultaneous formation of the new C1–C6 bond leading to the interrupted product **2** as shown in black on the energy profile in Figure 1. Based on the reported mode of action of a gold catalyst on a non-aromatic Cope reaction,[14] the $(CH_3)_3PAu(I)$ catalyst model was positioned above the C5–C6 double bond of **1a** (other positions were carefully examined, but found to be less favorable, see Figure S1 in Supporting Information). In the presence of the gold catalyst, a stepwise mechanism emerged from our calculations as illustrated on Figure 1 (green line), with the rate-limiting barrier being substantially reduced from 40.0 to 18.9 kcal.mol^{-1} for **1a**.

As gold significantly decreases the activation energy (~20 kcal.mol^{-1}), reaction rate should increase for the [3,3]-sigmatropic rearrangement. From a mechanistic perspective, gold achieves a decoupling of the C1–C6 bond formation (via TSA) from the subsequent C3–C4 bond cleavage (via TSB) occurring very quickly after a six-membered ring intermediate INT is formed. These new theoretical results extend previous literature[14,16] on non-aromatic Cope reactions to the Aromatic Cope reaction. A particularly noteworthy feature of the gold-assisted mechanism is the existence of a 6-membered ring intermediate (INT) stabilized by the substantial interaction between the gold atom and carbon C5 (otherwise negatively charged). This critical interaction was clearly revealed by the Independent Gradient Model (IGM) analysis[17] (δg^{peak} = 0.23 a.u., Intrinsic Bond Strength Index (IBSI) (C5…Au)=0.33) and Electron Localization Function (ELF) analysis[18] (see Figure S3 in SI), corroborating the existence of an Au–C5 bond (a weak metal coordination) in this intermediate. We also carefully tested the possibility of the gold binding the oxygen atom of the ester function at the intermediate INT. But this results in a 10 kcal.mol^{-1} less stable intermediate. For **1a**, the introduction of gold as a catalyst appears to effectively address one of the two key limitations of this reaction: the kinetic impediment for the [3,3]-rearrangement. However, this initial step still suffers from the inherent endergonicity of breaking aromaticity. Nevertheless, since the subsequent [1,3]H-shift of the ArCope cascade restores aromaticity, the whole transformation could potentially be thermodynamically favorable. Then, provided that the second step (proton transfer) is not rate limiting, it might be possible to observe the aromatic Cope reaction under milder conditions. As our previous study of the [3,3]-rearrangement under thermal conditions[12b] showed that the simultaneous introduction of a phenyl group at C4 and an ester group at C5 induces a significant 9 kcal.mol^{-1} lowering on both the energy barrier and the free energy of reaction, making this initial step exergonic, we evaluated these substitutions (R^1=CO_2Me and/or R^2=Ph) on the energy profiles with gold catalyst. Calculations on **1b, 1c** and ***(R, S)*-1d** have shown similar beneficial effects in the presence of gold (see Figure 1). The phenyl group appears to contribute to the driving force (exergonicity), while the ester function still lowers the barrier of the rate-limiting step. This primary theoretical exploration demonstrated that the prerequisites for observing the aromatic Cope reaction under mild conditions are met in the presence of gold(I).

2.2. Optimization and Scope.

Guided by these calculations (Figure 1), we started investigating gold-catalyzed ArCopeR with the predicted most favorable substrate, i.e. C4-phenyl and C5-methylester substituted α-allyl-α'-benzofuran γ-lactone **(±)-(*R,S*)-1d** (Table 1).[19] The latter was mixed in dichloromethane in the presence of 5 mol% triphenylphosphine gold(I) chloride and silver(I) hexafluoroantimonate. After 24 h, we were pleased to observe high conversion of **(±)-(*R,S*)-1d** into the expected ArCope product ***(E)*-3d** (91%) *at room temperature* as a single diastereomer in sharp contrast with the reaction performed thermically at reflux in toluene (16 h at 110°C) where the interrupted ArCope product ***(E,E)*-2d** was obtained in 79% yield[12b] (Entry 1 vs 2). Heating the reaction at 40°C achieved full conversion using the more electrophilic $(p CF_3Ph)_3PAuSbF_6$ catalyst in only 5 h and the compound ***(E)*-3d** was isolated in 96% yield while a minor amount of starting material remained untouched with triphenyl

phosphine ligand (Entry 3 vs 4). Other classical ligands used in gold catalysis[20] were clearly less efficient (Entries 5-7), despite that N-Heterocyclic Carbene (NHC) gold(I) catalyst selectively afforded the interrupted product ***(E,E)*-2d** (33%, entry 7). Control experiment revealed that silver hexafluoroantimonate used to generate the catalytically active gold(I) complexes was not able to promote the reaction (Entry 8).

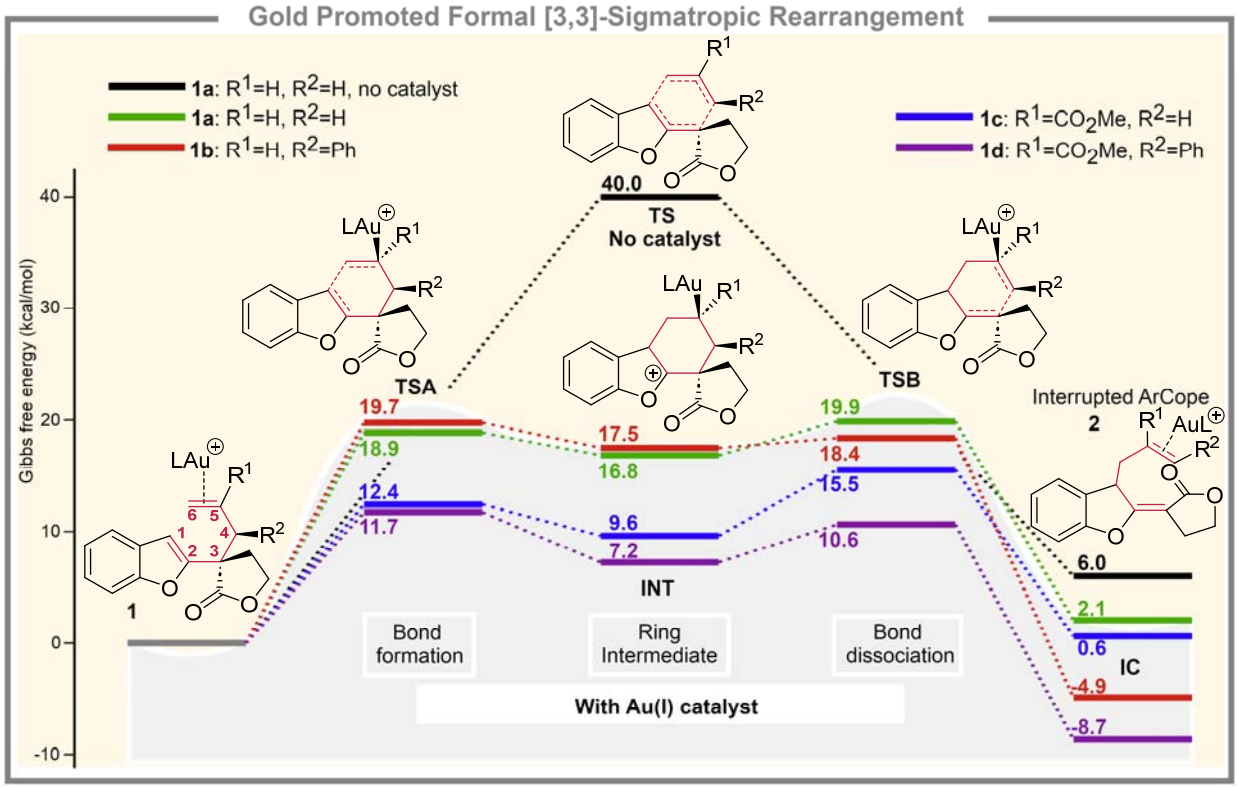

Figure 1. Free energy profiles obtained at 40˚C from DFT calculations at the PCM(DCE)-PBE0/SDD level of theory for the catalyzed system **1a-1d** and at the PCM(toluene)-M06-2X-D3/6-311++G(2d,2p)//PCM(toluene)-M06-2X/6-31+G* level of theory for the uncatalyzed reaction (**1a** = black). L stands for $P(Me)_3$. The pathway P1 including a chair-pro-*E* approach is the most favorable, see Figure S2 in SI for more details on the four possible pathways P1-P4. Energies are given relative to **1a** without gold catalyst (black) or relative to **1a** or **1b** or **1c** or **1d** with gold catalyst bound to the initial substrate (colored lines).

Table 1. Optimization Study on α-Allyl-α'-Benzofuran γ-Lactone **(±)-(*R,S*)-1d**.

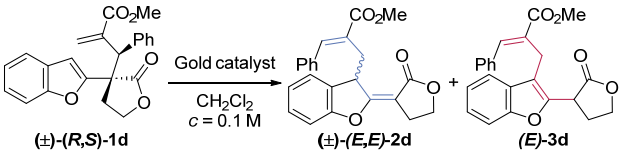

Entry	Catalyst (mol%)	Ag Salt 5 mol%	T (°C)	Time (h)	**2d**[a] (%)	**3d**[a] (%)
1	PPh_3AuCl (5)	$AgSbF_6$	rt	24	-	91
2[b]	-	-	110	16	90 (79)[c]	-
3	PPh_3AuCl (5)	$AgSbF_6$	40	5	-	96 (94)[c]
4	$(p\text{-}CF_3Ph)_3PAuCl$	$AgSbF_6$	40	5	-	100 (**96**)[c]
5	$(RO)_3PAu(MeCN)SbF_6$[d] (5)	-	40	7	49	7
			40	48	-	77
6	CyJohnPhos $(MeCN)SbF_6$ (5)	-	40	24	2	17
7	IPrAu(MeCN)SbF_6 (10)[e]	-	40	24	33	-
8	-	$AgSbF_6$	40	24	-[f]	-

[a]Calculated conversion from ^1H NMR integration of the crude mixture (*dr* 97/3). [b]Reaction performed at reflux in toluene, no reaction occurs below such temperature.[12b] [c]Isolated yield. [d]$P(OR)_3$ = *tris*(2,4-di-*tert*-butylphenyl)phosphite. [e]IPr = 1,3-bis(2,6-diisopropylphenyl)imidazol-2-ylidene. [f]No conversion.

To probe the exergonic significance of the C4-phenyl substitution on the gold(I)-catalyzed ArCopeR (Figure 1, blue vs purple profiles), we evaluated our optimal conditions (Conditions A, Table 1, entry 4) on the C5-ester α-allyl-α'-benzofuran lactone **1c** (Table 2). The reaction performed at 40°C provided the ArCope product **3c** but with a low conversion (30%) even after 24 h (Entry 1). Increasing the temperature at 70°C in dichloroethane (DCE) instead of dichloromethane with $(p\text{-}CF_3Ph)_3PAuSbF_6$ or $Ph_3PAuSbF_6$ catalysts clearly improved the efficiency of the transformation but failed to reach completion presumably through catalyst degradation with time (Entries 2 & 3). We then screened various solvents (see Table S1 in SI), and we found that hexafluoroisopropanol (HFIP), which has recently been used as activator through hydrogen bonding in gold catalysis,[21] afforded full conversion at 70°C in seal tube with high isolated yield of compound **3c** (90%, entry 4). A short survey of classical

counterions used in gold catalysis[22] (Entries 5-7) revealed that TfO^- was slightly better than SbF_6^-. Of note, compared to the thermal version (mesitylene at 165°C, entry 7 vs entry 6), **3c** was clearly obtained under milder reaction conditions. Control experiments demonstrated that the reaction did not occur thermically at 70°C in HFIP (Entry 9), nor with the AgOTf alone (Entry 10). As HFIP was able to generate active gold catalyst from gold(I) chloride precatalyst,[21b] we also performed the reaction in the presence of (pCF$_3$Ph)$_3$PAuCl without silver activator and we did not observe any conversion (Entry 11). The second round of optimization with **1c** thus led to a new set of conditions, i.e. 5 mol% of (p-CF$_3$Ph)$_3$PAuCl and AgOTf in HFIP at 70°C (Conditions B, Table 2, entry 6) which were applied to a gram scale reaction starting from **1c** affording **3c** in 85% yield.

Table 2. Optimization Study on C4-Unsubstituted α-Allyl-α'-Benzofuran γ-Lactone **1c**.

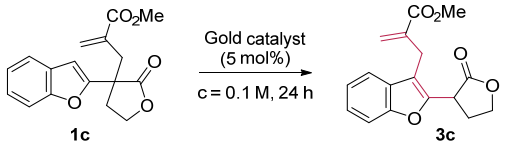

Entry	Gold Complex	Ag Salt 5 mol%	T (°C)	Solvent	**3c**[a]
1	(p-CF$_3$Ph)$_3$PAuCl	$AgSbF_6$	40	CH_2Cl_2	30
2	(p-CF$_3$Ph)$_3$PAuCl	$AgSbF_6$	70	DCE	62
3	PPh_3AuCl	$AgSbF_6$	70	DCE	59
4	(p-CF$_3$Ph)$_3$PAuCl	$AgSbF_6$	70	HFIP	100 (90)[b]
5	(p-CF$_3$Ph)$_3$PAuCl	$AgBF_4$	70	HFIP	98
6	(p-CF$_3$Ph)$_3$PAuCl	AgOTf	70	HFIP	100 (**91**)[b]
7	(p-CF$_3$Ph)$_3$PAuNTf$_2$	-	70	HFIP	23
8[c]	-	-	165	Mesitylene	88[b]
9	-	-	70	HFIP	-[d]
10	-	AgOTf	70	HFIP	trace
11	(p-CF$_3$Ph)$_3$PAuCl	-	70	HFIP	-[d]

[a]Calculated conversion from ^{1}H NMR integration of the crude mixture. [b]Isolated yield. [c]Reaction performed thermally in mesitylene.[12b] [d]No conversion.

We then explored the scope of the gold(I)-catalyzed ArCope reaction using condition B (Scheme 2). First, we assessed the stereoselectivity outcome of the transformation. Starting from the two diastereoisomers **(±)-(*R*,*S*)-1d** and **(±)-(*S*,*S*)-1d**, we observed a diastereodivergence of the reaction with the highly selective formation of **(*E*)-3d** and **(*Z*)-3d**, respectively, in excellent yields even using conditions A despite longer reaction times. The impact of the aromatic ring substitution in C4 on the reaction was then evaluated with α-benzofuran γ-lactones **1e-k**. Whatever the electron-withdrawing or electron-donating groups in different positions on this aromatic substituent, the ArCope products **3e-k** were obtained in excellent yields and high diastereoselectivities (83-96%). It was noticed that the electron-donating groups accelerated the reaction (**1g** (pOMe) converted in 1h vs **1f** (pNO$_2$), 5 h). The variation of the C5 substitution (R^1) was then investigated. Switching the methyl ester to nitrile group (**1l**, R^1=CN) clearly decreased the reaction rate and yield (**3l**, 53% in 72 h) but along with a loss of diastereoselectivity due to isomerization of the product during the reaction. Presumably, the sequestration of the catalyst by the nitrile group could be responsible for this lower efficiency. More challenging compound **1b** (see Figure 1) without the ester function (R^1=H) only afforded degradation products in conditions B, while adjusting the temperature to 40°C in DCE (conditions A) allowed the formation of the ArCope product **(*E*)-3b** in correct 54% yield, but once again with an *in-situ* isomerization of the double bond formed. The substrate **1a** with unsubstituted allyl group (R^1=R^2=H) unexpectedly failed to furnish ArCope product **3a** despite the significant reduction in activation barriers facilitated by gold (Figure 1, green profile) and was fully recovered after 48 h of reaction. The γ-lactone was then replaced by a methyl malonate moiety (substrates **1m-p**). Malonate motifs were known to decarboxylate or lead to abnormal ArCope products upon thermal reaction conditions.[10,11] However, this modification did not impact the rearrangement, and the products **3m-p** were obtained in good to high selectivity and yields (70-98%). Once again, the presence of a nitrile group on **1o** strongly decreased the catalytic activity, the ArCope product being obtained in 48 h but with good yield of 87%. Other heteroaromatic derivatives **1q-1z** were also evaluated such as (benzo)thiophene or indole. While the benzothiophene compounds **3q-r** were obtained in excellent yields and selectivity, the thiophene substrates **1s** and **1t** led to degradation and only 3% of **3s** could be isolated while **3t** was not found in the reaction crude. Free NH-indole motif on lactone or malonate substrates **1u-y** was perfectly compatible with our reaction conditions A affording ArCope products **3u-y** in 63-84% yield. Impressively, reaction times were drastically decreased in this series as illustrated by the formation of **3v** in only 5 min, while the benzofuran analog **3c** took 24 h to be obtained. Even more remarkable was the possibility to perform the reaction with unsubstituted α-allyl chain on γ-lactone and ethyl malonate derivatives **1w** and **1y** (R^1, R^2 = H) giving respectively ArCope **3w** and **3y** in good yields. The rearrangement of **1w** was also performed at room temperature and afford **3w** in 65% for 7 h while the thermal reaction laboriously gave 24% of yield at 165°C in mesitylene after 48 h.[12b] Such results contrast with benzofuran substrate **3a**, which was totally unreactive upon gold catalysis, but also with the recent report of Grenning using engineered N-triflate indole derivatives to obtain interrupted Cope products.[8a] Finally, the N-methyl indole derivative **1z** was also successfully engaged in the ArCope leading to **3z** in only 20 min.

2.3. Extended Theoretical Investigation

Diving deeper into the mechanism. Our preliminary DFT calculations predicted that gold catalysis would significantly enhance the reaction rate of the primary formal [3,3]-sigmatropic rearrangement for **1a-d** substrates (see Figure 1). However, discrepancies between theory and experiment suggest that the mechanism depicted in Figure 1 cannot fully account for the experimental findings. For instance, while the unsubstituted substrate **1a** (R^1, R^2=H) exhibits a relatively low barrier of 18.9 kcal.mol^{-1} for the entrance channel on Figure 1 (normally readily overcome at 40°C, $t_{1/2}$ = 1.7s), this reaction is experimentally not

observed in the presence of gold. The unexpected lack of reactivity for **1a** prompted us to better understand the actual mechanism at play. To begin with, we extended the reaction pathway of Figure 1 to encompass the entire process, including the subsequent [1,3]H-shift up to the final ArCope

product. The latter species **3a** is found to be stable relatively to **1a** ($\Delta G°$=-4.6 kcal.mol^{-1}, see Figure 2 and Figure S4), suggesting that kinetic limitations are in fact the primary obstacle.

Scheme 2. Aromatic Cope Reaction Scope.

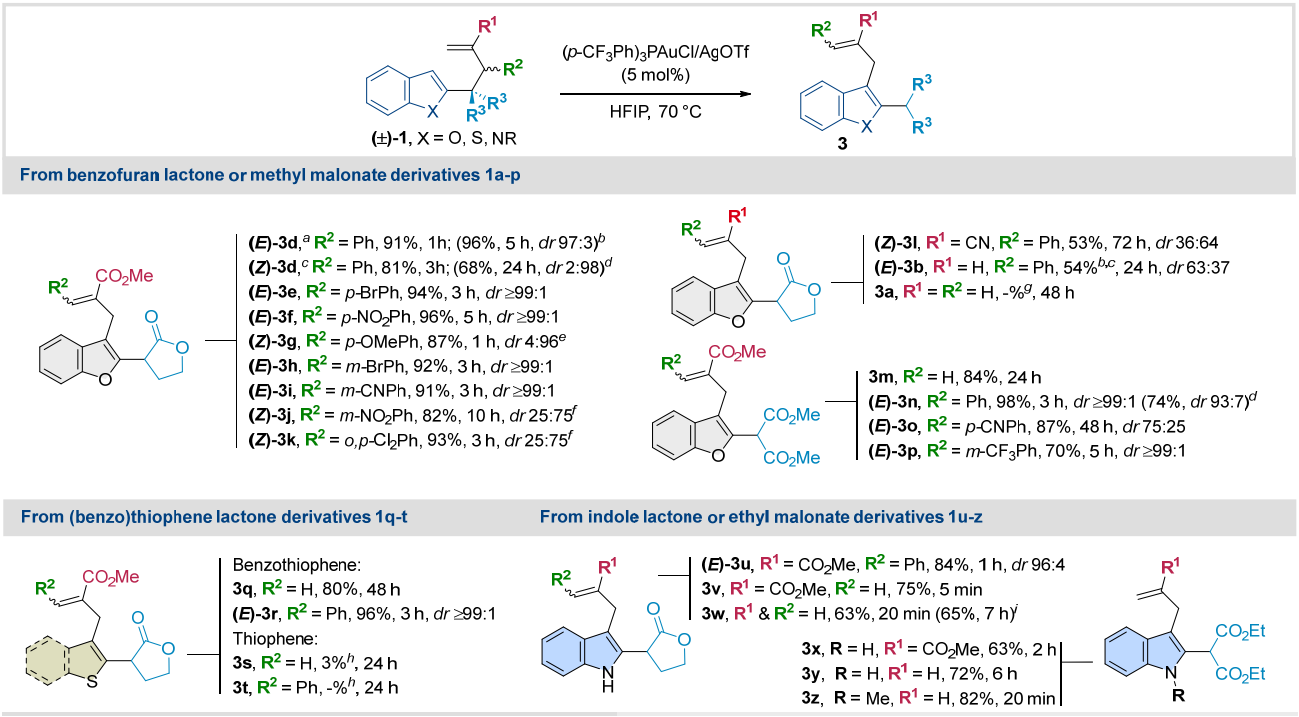

[a]Starting from **(*R*,*S*)-1d**: *dr* (*E*:*Z*) = ≥99:1. [b]Run with $AgSbF_6$ activator at 40°C in CH_2Cl_2 (Conditions A). [c]Starting from **(*S*,*S*)-1d**: *dr* (*E*:*Z*) = 3:97. [d]Run with $AgSbF_6$ activator at 70°C in DCE. [e]Run at 40°C. [f]Starting from derivatives **1j,1k** with the corresponding diastereomeric mixture *R*,*S*/*S*,*S*. [g]No conversion. [h]Degradation occurs. [i]Run at room temperature.

The general profile obtained for **1a**-**1d** is sketched on Figure 2 (in grey color). Following the formal [3,3]-sigmatropic rearrangement, the subsequent [1,3]H-shift is crucial for the re-aromatization. It is important to bear in mind that without a relay to facilitate this [1,3]H-shift, this elementary reaction is unlikely to proceed efficiently. In this study, given the absence of external bases and acids, we assumed that it can potentially occur intramolecularly via a two-step mechanism starting from the interrupted Cope intermediate **2** (IC → ENOL → PRODUCT). The first step: a sigmatropic [1,5]H-shift, involves the C3-lactone to transfer the proton from C1 to the carbonyl oxygen (TSPT1, forming the enol on Figure 2), before its final destination at the C3 carbon in **3**. The presence of an electron-withdrawing group at C3 (the lactone here) has been previously reported as a structural feature that can circumvent the unfavorable [1,3]H-shift in ArCope, facilitating the tautomerization back to the aromatic system.[4] However, while this pathway is theoretically possible for **1a**, the too large activation barrier of 32.8 kcal.mol^{-1} via TSPT1 predicted for this first step ([1,5]H-shift from C1 to O) precludes the reaction at 40°C. Gold(I) has no effect on this barrier. This unfavorable activation energy also applies to the reaction of compound **1d** (R^1=CO_2Me, R^2=Ph, $\Delta G°^{\ddagger}$=31.6 kcal.mol^{-1}, see Figure 2 and Figure S4), which, despite this, is experimentally observed, again highlighting a discrepancy between the postulated mechanism and experiment. In fact, examination of **1a-d** invariably reveals the presence of this very large [1,5]H-shift energy barrier in the exit channel (in the range 31.6 to 34.2 kcal.mol^{-1}), theoretically prohibiting any global [1,3]H-shift at 40°C (and then re-aromatization) from the interrupted ArCope intermediate **2** (IC).

An alternative re-aromatization pathway mediated by Au(I) and starting from intermediate **2a** (interrupted Cope) was investigated. In this scenario, the Au(I) catalyst was positioned at the C2=C3 double bond to facilitate the [1,5] proton transfer by weakening the C1-H bond (see Figure S8 in ESI). Our findings indicate however a calculated free energy barrier of 29.8 kcal/mol at 313K, within the range of large barriers previously reported for this proton transfer starting from **2**.

To summarize, all substrates exhibit a too high energy barrier for re-aromatization from **2** (IC), but nevertheless some react. The Lewis acidic nature of the Au(I) complex could potentially lead to the formation of Brønsted acidic species, which could catalyze the re-aromatization via protonation of the lactone carbonyl oxygen and generating a positive charge on C2, thereby facilitating re-aromatization through proton loss from C1. However, this should apply to all substrates, including **1a** that does not react. Furthermore, experimental tests involving the deliberate addition of acid to the reaction mixture **1a** did not induce the desired transformation. That is the reason why our theoretical investigation

continued to primarily examine intra-molecular processes in DCE.

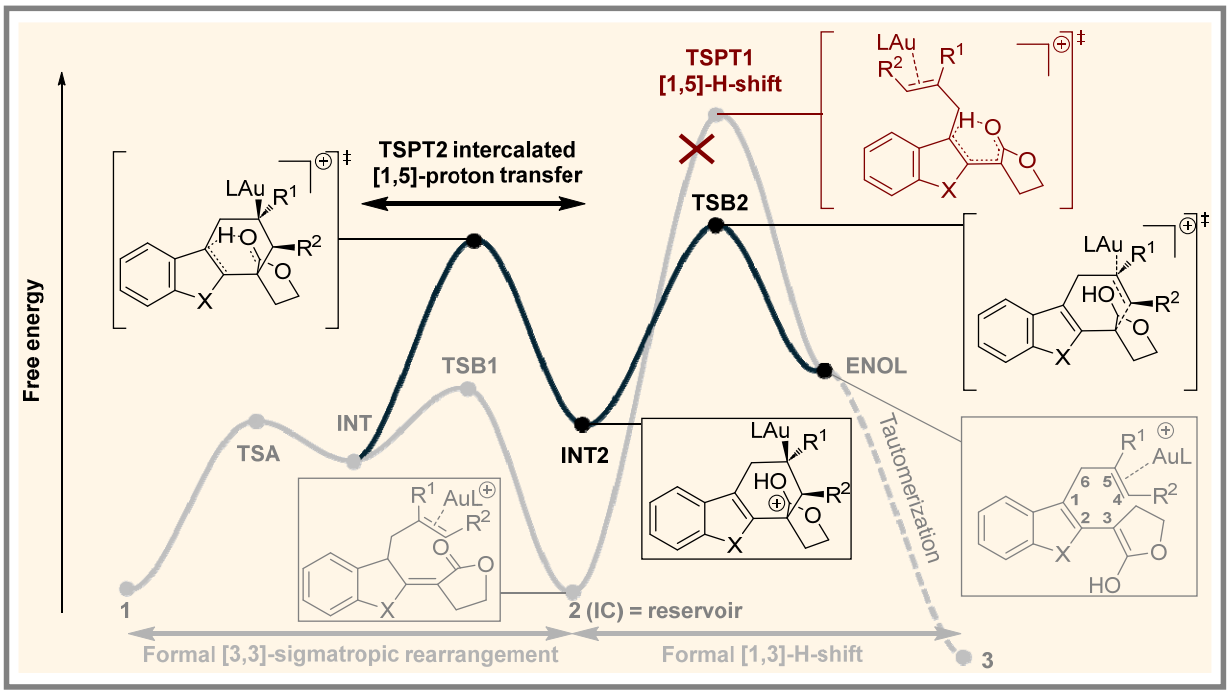

1	X	R¹	R²	Catalyst	ΔG°313K (kcal.mol⁻¹) TSA	INT	TSB1	2	TSPT1	TSPT2	INT2	TSB2	ENOL	3
Lactone derivatives														
1a	O	H	H	Me₃PAu(I)	18.9	16.8	19.9	2.1	34.9	35.1	20.9	31.3	12.9	-4.6
1b	O	H	Ph		19.7	17.5	18.4	-4.9	26.9	32.8	20.1	27.5	5.1	-11.2
1c	O	CO_2Me	H		12.4	9.6	15.5	0.6	34.8	26.0	12.2	27.0	17.1	-3.1
1d	O	CO_2Me	Ph		11.7	7.2	10.6	-8.7	22.9	21.3	8.1	19.7	7.0	-13.8
1q	S	CO_2Me	H		12.8	9.7	14.9	1.44	34.9	24.1	10.5	26.7	18.2	-1.4
1r	S	CO_2Me	Ph		10.8	6.6	10.1	-9.8	22.4	17.4	6.5	17.2	7.2	-12.6
1w	NH	H	H		11.9	3.4	12.5	0.4	32.0	26.9	20.9	30.8	13.7	-6.0
1v	NH	CO_2Me	H		6.4	-5.1	8.1	-0.7	31.7	17.4	11.3	26.6	16.9	-4.0
1c	O	CO_2Me	H	IPrAu(I)	14.4	10.6	16.7	0.8	34.7	28.0	13.1	27.4	17.8	-2.9
1d	O	CO_2Me	Ph		12.3	8.4	9.3	-12.7	20.5	21.2	8.8	17.8	3.8	-16.2
Malonate derivatives														
1m	O	CO_2Me	H	Me₃PAu(I)	14.1	11.0	16.8	1.1	29.3	27.4	7.8	21.6	13.6	-3.9
1n	O	CO_2Me	Ph		12.6	9.1	13.1	-10.5	17.0	22.0	5.6	14.8	1.9	-17.5

Figure 2. General free energy profile for the Au(I)-catalyzed system; the formal [3,3]-sigmatropic rearrangement/[1,3]H-shift cascade for lactone derivatives: 1→2→3 is in grey color and an alternative reaction mechanism is unveiled in black color; two competing pathways exist from INT species; L stands for P(Me)₃. Bimolecular transition state for the final tautomerization step is not described in this study. Gibbs free energy values (relative to reactant) for each stationary point along examined energy profiles for the pathway P1 (Figure 1) and alternative pathway P2; DFT calculations at the PCM(DCE)-PBE0/SDD level of theory.

We then decided to explore the possibility for the proton to be transferred upstream from IC, directly from the previous intermediate INT, through an [1,5]-proton transfer (TSPT2), towards INT2, postponing the C3-C4 bond breaking (TSB2). The so-called "intercalated H-shift"competing pathway reported in black on Figure 2 (INT → INT2 → ENOL) emerges from this exploration. Remarkably, starting from INT, the [1,5]-proton transfer from C1 to the lactone involves now substantially lower barriers via TSPT2, in the range of 14.1-16.4 kcal.mol^{-1} for **1b-d** and 18.3 kcal.mol^{-1} for **1a**, with the latter being kinetically unfavored compared to the other substrates (see Figure 3). Once this step is overcome, the key to the remaining mechanism lies in the subsequent cleavage of the C3-C4 bond and does not require much energy (INT2 → ENOL, Figures 2 and 3). It must be noted that the final tautomerization back to the aromatic benzofuran likely involves the assistance of another molecule to overcome the high energy barrier generally associated with tautomerization. Experimental observations strongly suggest that this last step is not rate-determining. Indeed, we experimentally observe that the overall rate depends on C4 and C5 substituents, while, from a mechanistic

point of view, the tautomerization reaction proceeds independently of these substituents. Hence, elucidating the transition state of the final bimolecular tautomerization step was not achieved in the present study. For practical purposes, for kinetic calculations (see below), a non-rate-limiting barrier of 2 kcal.mol^{-1} was employed.

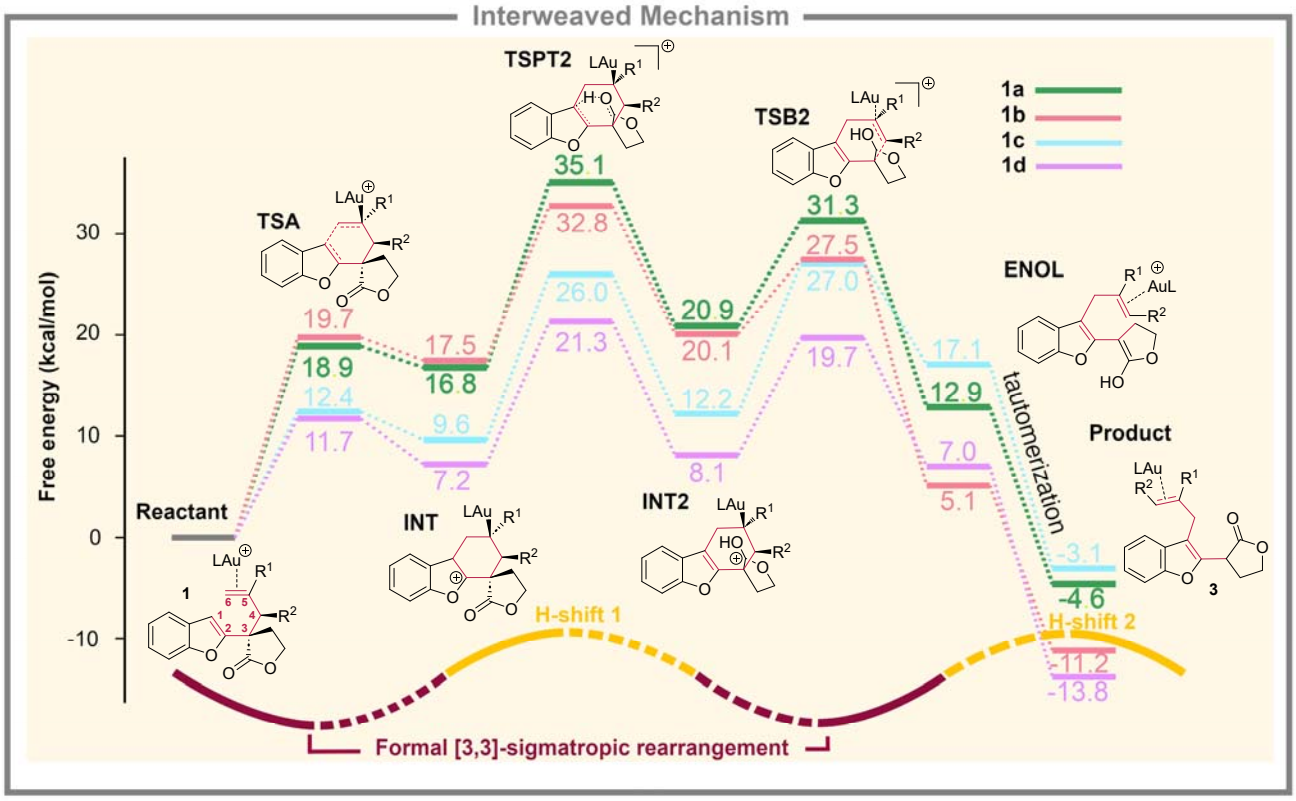

Figure 3. Gibbs free energy profiles obtained at 40°C from DFT calculations at the PCM(DCE)-PBE0/SDD level of theory for the catalyzed systems **1a-d**; L stands for P(Me)$_3$; Bimolecular transition state for the final tautomerization step not described within this study.

Thus, DFT calculations suggest two competing pathways from INT: either the intercalated [1,5]-proton-transfer (via TSPT2) or the immediate formation of the interrupted Ar-Cope product IC (via TSB1). Initially, the latter is clearly favored due to its lower barrier from intermediate INT. However, it leads to a dead end (too large subsequent TSPT1 height for [1,5]H-shift), while the other channel (the early [1,5]proton-transfer from INT) presents an initial higher barrier (E(TSPT2) > E(TSB1)) but a more favorable overall reaction profile afterwards. It is important to consider that the reaction might also revert from the intermediate INT to the starting material, making it challenging to decipher the intricacies of this complex mechanism solely by examining barrier heights. That is the reason why a numerical simulation of a kinetic model based on our DFT data was meticulously carried out to obtain the time evolution of the reacting systems **1a-d**, starting with the reactant at an initial concentration of 0.1 mol.L^{-1} (see Figure S5 in SI). While the inherent limitations in quantum chemistry accuracy (2-3 kcal.mol^{-1} for DFT in general[23]) and the use of a simplified catalyst model employed here restrict the quantitative scope of such kinetic numerical simulations, they nevertheless provide qualitative trends in the reaction behavior. The results provide clear evidence that compound **1a** exhibits by far the slowest kinetics among all the compounds (see Figure S5), suggesting no reactivity, in line with experimental findings. Furthermore, these kinetic simulations, supported by energy profiles (Figures 3 and S4), clearly demonstrate that the presence of the ester function at C5 significantly facilitates the reaction. This is in full agreement with the experimental observations for compounds **1c** and **1d**, which exhibit markedly faster reaction rates compared to their C5-unsubstituted counterparts **1a** and **1b**. This finding also aligns perfectly with our previous results on the uncatalyzed reaction.[12] Both studies concur that a properly positioned donor-acceptor pair at C2 and C5 in the Cope rearrangement enhances the push-pull electronic effect, which acts as the kinetic driving force for the Cope reaction. Noteworthy, kinetic modeling shows that the interrupted Ar-Cope product acts as a transient reservoir (see Figure 2) feeding the competing intercalated H-shift, specifically when phenyl is present. This behavior is attributed to the increased stability of the IC product, resulting from additional π-delocalization with the newly formed C4=C5 double bond and from C3–C4 steric decongestion upon C3–C4 bond cleavage. This suggests that if this interrupted product were significantly further stabilized, it could become a kinetic trap, disfavoring the overall Cope rearrangement, yielding the interrupted Cope product (see the discussion below).

To summarize, in the absence of catalyst, the [3,3]-sigmatropic rearrangement is the rate-limiting step of the ArCope reaction. The use of gold (with no base in the medium) changes the game by enabling a faster [3,3]-sigmatropic transformation and moreover facilitating the re-aromatization through an intercalated [1,5]-proton transfer, which now interweaves with the [3,3]-sigmatropic rearrangement. Our analysis suggests that the reaction first proceeds through the formation of intermediate **2** (IC). Then, if **2** is not excessively stabilized, it is not trapped and it can potentially undergo a competing [1,5]-proton transfer mechanism, "backtracking" from **2** (IC) to INT. This new mechanism reconciles the observed experimental results with theoretical predictions for the gold-catalyzed reaction.

Possible assistance of HFIP solvent. To limit the computational efforts and avoid excessive calculation time, all theoretical studies were conducted in the implicit solvent DCE, mirroring the initial experimental solvent in Table 2. Experimentally, while HFIP demonstrated improved performance overall (Table 2), no significant enhancements were however observed for compound **1a** (Scheme 2). Yet, HFIP is a strong hydrogen bond-donating solvent[24] and a HFIP-mediated mechanism might in principle accelerate the [1,5]-proton transfer identified as limiting by theoretical calculations.

Complementary classical molecular dynamics simulations with an explicit solvent environment revealed a significant energetic penalty associated with orienting HFIP molecules for an efficient solvent-mediated proton transfer (see Figure S6 of the radial distribution functions reported in the Supporting Information). Accurately capturing the explicit solvent effects on the reaction barrier involving HFIP-mediated proton transfer would necessitate meta-dynamics simulations to directly sample the free energy landscape of this process. Such calculations are beyond the scope of this study. Nevertheless, the proposed *interweaved shifts* mechanism remains the most plausible explanation for the observed differential reactivity of compound **1a**, with the origins of this discrepancy likely rooted in the early stages of the reaction (TSPT2, TSB2 on Figure 3).

Effect of Malonate at C3. DFT calculations highlight very similar energy profiles for γ-lactone substrates **1c**, **1d** and malonate derivatives **1m**, **1n** (see Figure 2). Notably, an identical trend is observed regarding the effect of the phenyl at C4 on the stabilization of the interrupted ArCope product IC (-10.5 kcal.mol^{-1}) and rearomatized product (-17.5 kcal.mol^{-1}). This finding strongly still supports our belief that, depending on the substrate, the interrupted ArCope product IC might be trapped and isolated under specific experimental conditions (see the discussion below).

Ring modulations. Curious about the impact of a different heterocycle than benzofuran on the reaction, we conducted theoretical investigations on four additional reactions: two involving benzothiophene derivatives and two involving indole heterocycles (see Figure 2). The benzothiophene derivatives **1q** (R^1=CO_2Me, R^2=H) and (±)-(***R*,*S***)-**1r** (R^1=CO_2Me, R^2=Ph) behave very similarly to their corresponding oxygenated compounds **1c** and **1d**, respectively, in agreement with experimental yields. Once more, the presence of the phenyl group at C4 makes the [3,3]-rearrangement significantly exergonic at 40°C (-9.8 kcal.mol^{-1}).

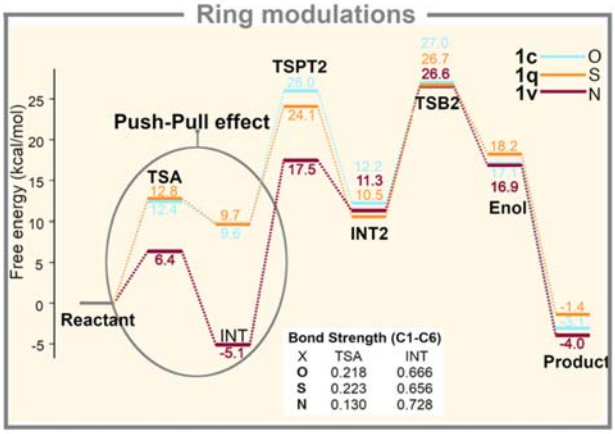

Figure 4. Free energy profiles obtained at 40°C from DFT calculations at the PCM(DCE)-PBE0/SDD level of theory for the catalyzed systems **1d, 1q** and **1w** (R^1=CO_2Me, R^2=H); L stands for $P(Me)_3$; the bond strength between C1 and C6 was assessed by means of IGM/IBSI index.

α-Indolyl γ-lactone derivatives **1v** (R^1=CO_2Me, R^2=H) and **1w** (R^1=H, R^2=H) promote a much more favorable entrance channel. Indeed, the activation barrier for the initial ring closure is reduced by about 6-7 kcal.mol^{-1} compared to the oxygenated species and the formation of intermediate INT is accompanied by a large stabilization (see Figure 4). It is worth noting that the 6-membered ring intermediate INT displays now exceptionally low energy (3.4 kcal.mol^{-1} for **1w**) and even surpasses the reactant stability for **1v** (with a value of -5.1 kcal.mol^{-1}) (see Figure 4).

These findings align perfectly with experimental observations (Scheme 2) demonstrating the enhanced reactivity of indole derivatives, even when unsubstituted. These remarkable results for indole derivatives prompted us to investigate the underlying electronic factors that contribute to this increased reactivity and overstabilization of the six-membered ring INT. To shed light on this, we assessed the bond strength (IGM/IBSI[17c]) of the newly formed bond C1-C6 in TSA and in the resulting 6-membered ring INT (see Figure 4). Our results reveal that the presence of nitrogen substantially strengthens the newly formed bond C1-C6 in INT, thereby significantly stabilizing the new 6-membered ring for the indole derivative. This is very likely connected to the nitrogen's electron-donating properties, enhancing the push-pull effect previously mentioned, compared to oxygenated species. In line with this, the IGM/IBSI analysis of TSA emphasizes an early TS for the indole derivative (the bond strength required to reach TSA is less drastic in this case).

2.4. Interrupted Aromatic Cope Reaction

Overall, the theoretical analysis suggests that interrupted Cope product **2** could be stable enough to be isolated. In this way, we noticed during the optimization work (Table 1, entry 7) that the use of NHC-gold(I) catalyst led to a selective reaction in favor of the dearomatized compound,[25] i.e. the interrupted ArCope product **(*E*,*E*)-2d** obtained from **(±)-(*R*,*S*)-1d**,[8a,26] despite the low conversion in DCM. These results prompted us to optimize the dearomative Cope reaction (see SI, Table S2). We found that the rearrangement performed in HFIP with 5 mol% of $IPrAuNTf_2$ at 40°C

(Conditions C) was particularly chemoselective giving 88% conversion of racemic **(*E*,*E*)-2d** and only 4% of the ArCope product **(*E*)-3d**. Such divergent gold reactivity controlled by the catalyst[27] was then briefly exemplified (Scheme 3). Starting for highly enantioenriched **(–)-(*R*,*S*)-1d**, we were able to obtain selectively the interrupted product **(*R*,*E*,*E*)-2d** in only 3 h compare to 16 h at 110°C (Table 1, entry 2) and isolate it with an excellent yield of 87%. However, a modest enantiomeric ratio of 62:38 was unexpectedly obtained while the chirality transfer was highly efficient in thermal version.[12] The same trend was observed for benzofurans derivatives **(*R*,*E*,*E*)-2e** and **(*R*,*E*,*E*)-2h**, with respectively *p*-Br and *m*-Br substituent on aromatic ring at C4 position. To get insight in the loss of enantioselectivity during the process, we carried out control experiments starting from chiral **(*R*,*E*,*E*)-2e** (see Chart S1 in SI). We found that the racemization occurred after the ArCope rearrangement and only in the presence of both gold(I) catalyst and HFIP. Fortunately, this phenomenon was specific to the benzofuran series as a complete chirality transfer was achieved with the benzothiophene derivative **(*R*,*E*,*E*)-2r**.

Scheme 3. Dearomative Cope rearrangement.

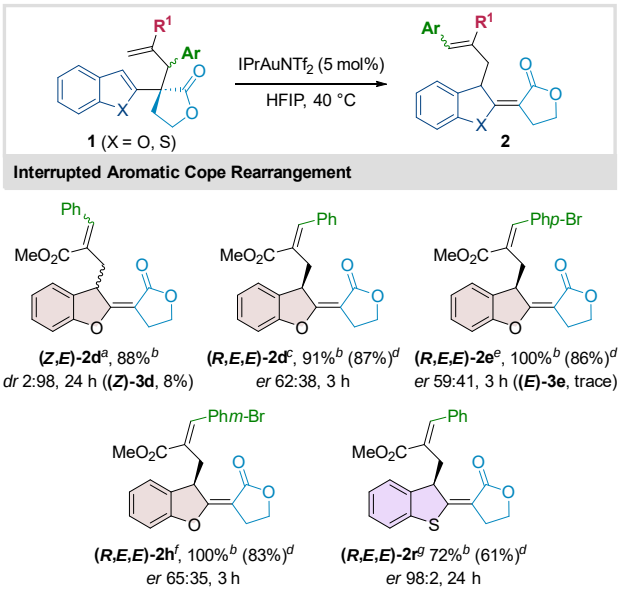

[a]Starting from racemic **(*S*,*S*)-1d**. [b]Calculated conversion form ^{1}H NMR integration of the crude mixture. [c]Starting from **(*R*,*S*)-1d** *er* 100:0. [d]Isolated yield. [e]Starting from **(*R*,*S*)-1e** *er* 97:3. [f]Starting from **(*R*,*S*)-1h** *er* 98:2. [g]Starting from **(*R*,*S*)-1r** *er* 98:2.

The use of the IPrAuNTf$_2$ catalyst (Scheme 3) instead of (*p*-CF$_3$Ph)$_3$PAu(I)OTf (Table 1, entry 4) leads to the formation of the interrupted Cope product **2d** (IC) rather than product **3d**, prompting us to investigate these striking experimental outcomes computationally. The general energy profile in Figure 2 might offer some clues regarding this mechanistic divergence. Indeed, the intermediate **2** (IC) on Figure 2 might be trapped if it were substantially stabilized. Hence, the combined analysis of experimental observations and of the theoretical energy profile suggests that IPrAuNTf$_2$ catalyst might significantly stabilize **2d** compared to the (*p*-CF$_3$Ph)$_3$PAu(I) catalyst. Our primary DFT calculations already pointed out the significant stabilization (-8.7 kcal.mol^{-1}) of this interrupted Cope product **2d** in the presence of the catalyst model [AuP(Me)$_3$]$^+$ when both phenyl at C5 and ester at C4 are present (Figure 2, entry 4). This stabilization is solely due to the presence of the phenyl group at C5 and is attributed to the development of a synchronized π-bridging upon forming the new double bond C4=C5 in **2d** (IC). Despite this, it appears that this stabilization is not sufficient to trap this intermediate as evidenced by the final observation of **3d** and not **2d** during experiment using (*p*-CF$_3$Ph)$_3$PAu(I) catalyst. Complementary DFT calculations carried out on **2d** in the presence of the IPrAu(I) catalyst revealed a significant extra-stabilization of more than 4 kcal.mol^{-1} for the interrupted Cope product **2d** (-12.7 kcal.mol^{-1}) compared to (*p*-CF$_3$Ph)$_3$PAu(I) (-8.1 kcal.mol^{-1} for actual catalyst), providing a mechanistic rationale for the experimental observation of **2d**. Such a pronounced stabilization likely traps **2d** (IC), preventing the re-aromatization to take place through the *interweaved* mechanism. The IGM analysis suggests that this enhanced stability can partly be attributed to van der Waals interactions taking place between the catalyst IPrAu(I) and the substrate along the reaction path (see Figure 5), highlighting the crucial role of these non-covalent interactions in modulating the reaction pathway.[28] The main difference between the two catalysts is that only IPrAu(I) can significantly engage in non-covalent interactions with the substituents at positions C4 and C5 in **2d**.

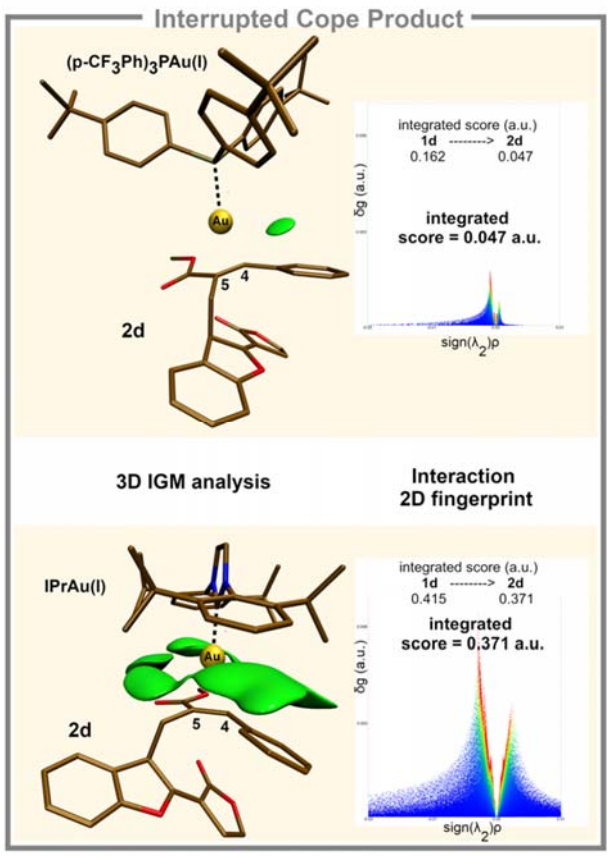

Figure 5. IGM analysis of non-covalent interactions taking place in the interrupted Cope product between substrate **2d** and catalyst (a) (*p*-CF$_3$Ph)$_3$PAu(I) (b) IPrAu(I), from DFT calculations at the PCM(DCE)-PBE0/SDD level of theory; fragment 1 = **2d** , fragment 2 = catalyst (minus the gold atom and its

directly coordinated atom); the same δg iso-value (0.001 a.u.) was used to compare catalysts on an equal footing; iso-surfaces are colored on a BGR scheme over the range -0.08 a.u. < sign(λ_2)ρ < + 0.08 a.u. (red, green and blue iso-surface regions are associated with non-bonded, van der Waals and attractive interactions. Hydrogen atoms are removed for the sake of clarity.

3. CONCLUSION

To summarize, we demonstrated that the introduction of gold(I) catalysis unlocks the aromatic Cope rearrangement, enabling the reaction at mild heating and even room temperature. Based on computational study, we developed a gold(I)-catalyzed ArCope reaction of α-allyl-α'-heteroaromatic γ-lactones or malonates, providing a direct and efficient access to CH functionalized aromatic molecules in excellent yields and high stereoselectivities. These results represent the first catalytic and synthetically useful protocol to promote ArCopeR in mild conditions (5 mol% of (*p*-$CF_3Ph)_3PAuCl$ and AgOTf in HFIP at rt to 70 °C). Theoretical calculations provided valuable insights into the reaction mechanism, showing that gold(I) triggers a triple effect: (a) it enhances the reaction rate through lowered activation energy, (b) it causes a stepwise [3,3]-sigmatropic process pinvolving the formation of an intermediate, (c) the latter entailing a novel gold-mediated pathway involving an intercalated proton transfer. The experiment aligning with theoretical predictions also demonstrated that a strategic positioning of a donor-acceptor pair at the C2 and C5 positions significantly enhances a push-pull electronic effect, acting as the key driving force for the reaction kinetics, notably in the benzofuran series. Moreover, the introduction of a group possessing a delocalizable π-system at C4 enhances the reaction exothermicity by extending the π-conjugation in the final product. In a divergent manner, the employment of an NHC-Au(I) catalyst enables the isolation of the dearomatized intermediate of the ArCope reaction from chiral scaffolds, with high stereoselectivity for benzothiophene derivatives. Quantum mechanical calculations shed light on the pivotal role of van der Waals interactions between the catalyst and substrate in stabilizing the intermediate and governing the latter reaction outcome. This possibility to stop the reaction at the dearomatization stage offers the prospect of developing novel molecular entities. Finally, our findings underscore the transformative potential of indole derivatives in gold-catalyzed ArCope reactions, offering a broader, more efficient, and streamlined synthetic approach. DFT and IGM analyses suggest that the indole nitrogen atom, through its electron-donating properties, strengthens the newly formed C1-C6 bond in the key intermediate, facilitating the process. Overall, this study represents significant advancement and understanding in the field of aromatic Cope rearrangements. The gold(I)-catalyzed ArCopeR offers a powerful tool for organic chemists to achieve C-H functionalization and create complex dearomatize molecules under mild conditions and with excellent stereocontrol. Moving forward, efforts are directed toward various aromatic skeleton to further extend our methodology.

4. EXPERIMENTAL SECTION

4.1. Computational Details.

Geometrical optimizations of minima and transition states (TS) were performed using DFT with PBE0[29] functional and SDD[30] basis set (Stuttgart/Dresden ECP) as employed in the Gaussian 16 package[31] (initial conformers were taken from our previous work[12b]). PBE0 was chosen due to its better accuracy towards 5d transition metal complexes.[32,33] A polarizable continuum model[34] (PCM) of Dichloroethane (DCE) was employed to account for solvation. The vibrational modes were analytically computed to check the absence of imaginary frequencies for local minima and the presence of one single imaginary frequency for TS. Intrinsic Reaction Coordinates (IRC) calculations were performed to check that each TS connects the respective minima. The reaction and activation Gibbs free energies were obtained at 313.15 K using KiSThelP program.[35] To assess the impact of the more realistic (*p*-$CF_3Ph)_3Au(I)$ catalyst on our computational results, we calculated reaction profiles for both species **1a** and **1c** using this catalyst and compared them to those obtained with the simpler $(Me)_3PAu(I)$ model. The results indicate that the energy profiles are only moderately affected by the catalyst change and suggest that the simplified model accurately captures the essential features of the reaction mechanism (see section 3.7 in ESI).

Independent Gradient Model (IGM)[17c] analyses were performed with IGMPlot program. Within the IGM-δg approach, the resulting δg iso-surfaces representing the interaction regions are colored according to the electron density (ED) value oriented with the sign of λ_2 (second eigenvalue of the ED Hessian). A BGR color code is used: blue for attractive, green for weak and red for non-bonding interactions. VMD software[36] was employed to generate the corresponding figures and iso-surfaces. ELF analyses were performed using TopChem2 program.[37]

The kinetic simulations were carried out with the numerical solver TENUA[38] to obtain the time evolution of the system reported on Figure S5, starting from the mixture containing initial substrate at 0.1 mol. L^{-1}. Due to the lack of kinetic data for the final tautomerization step, an arbitrary barrier of 2 kcal.mol^{-1} was assumed for the implementation of kinetic numerical simulations (time concentration profiles being unaffected by this arbitrary value). The Bader-Deuflhard algorithm was used to solve the differential equations.

4.2. General Methods for Aromatic and Interrupted Cope Reactions.

ArCope Procedure: In a seal vial, a solution of (4-$CF_3Ph)_3PAuCl$ (5 mol%) and $AgSbF_6$ (5 mol%) in distilled DCM or DCE (0.1 mol/L) (Conditions A) or (*p*-$CF_3Ph)_3PAuCl$ (5 mol%) and AgOTf (5 mol%) in distilled HFIP (0.1 mol/L) (Conditions B) was stirred for 15 minutes to form the catalyst species. The substrate **1** was then added and the mixture is heated and stirred at the given temperature (rt to 70°C). Once the reaction was complete the crude mixture was filtered over celite, concentrated and then purified by chromatography on SiO_2 to product **3**.

Interrupted ArCope Procedure: In a seal vial, $IPrAuNTf_2$ (5 mol%) and substrate **1** were dissolved in distilled HFIP (0.1 mol/L) (Condition C) and the mixture was heated and stirred at 40°C. Once the reaction was complete the crude mixture was filtered over celite, concentrated, and then purified by centrifugal thin-layer chromatography on SiO_2 to afford the product **2**.

ASSOCIATED CONTENT

Supporting Information.
The Supporting Information is available free of charge via the Internet at http://pubs.acs.org.
Supplementary Figures, Tables, and Charts. Detailed experimental procedures, spectral data for all compounds, and full theorical part. NMR data of pure compounds are available at https://doi.org/10.57745/AOFGB9.

AUTHOR INFORMATION

Corresponding Authors

Aurélien Blanc; orcid.org/0000-0003-4240-3281;
ablanc@unistra.fr
Emmanuel Riguet; orcid.org/0000-0002-8926-113X;
emmanuel.riguet@univ-reims.fr
Eric Hénon; orcid.org/0000-0001-9308-6947;
eric.henon@univ-reims.fr

Author Contributions

‡P.L. and A.R. contributed equally to this work.

Notes

Any additional relevant notes should be placed here.

ACKNOWLEDGMENT

We thank the French Agency of Research (ANR-22-CE07-0021, ArCopeRebirth), the CNRS, the universities of Strasbourg and Reims Champagne-Ardenne, the Communauté Urbaine du Grand Reims, and the French Ministry of Higher Education, Research, and Innovation for financial support. We gratefully acknowledge Delphine Hatey for the preparation of some gold precatalysts and Alexis Vallée for Chiral HPLC analysis. Thanks are given to the MaSCA (Maison de la Simulation de Champagne-Ardenne, France) and to the CRIANN computational center for computing facilities.

REFERENCES

(1) Cope, A. C.; Hardy, E. M. Introduction of Substituted Vinyl Groups. V. A Rearrangement Involving the Migration of an Allyl Group in a Three-Carbon System. *J. Am. Chem. Soc.* **1940**, *62*, 441–444.

(2) For selected reviews, see: (a) Nubbemeyer, U. Recent Advances in Asymmetric [3,3]-Sigmatropic Rearrangements. *Synthesis* **2003**, 961–1008. (b) Ilardi, E. A.; Stivala, C. E.; Zakarian, A. [3,3]-Sigmatropic Rearrangements: Recent Applications in the Total Synthesis of Natural Products. *Chem. Soc. Rev.* **2009**, *38*, 3133–3148. (c) Graulich, N. The Cope Rearrangement - the First Born of a Great Family. *Wiley Interdiscip. Rev. Comput. Mol. Sci.* **2011**, *1*, 172–190. (d) Lee, H.; Kim, K. T.; Kim, M.; Kim, C. Recent Advances in Catalytic [3,3]-Sigmatropic Rearrangements. *Catalysts* **2022**, *12*, 227.

(3) (a) Cope, A. C.; Field, L.; MacDowell, D. W. H.; Wright, M. E. Rearrangement of Allyl Groups in Three-Carbon Systems. VI. Benzene and Phenanthrene derivatives. *J. Am. Chem. Soc.* **1956**, *78*, 2547–2551. (b) Cope, A. C.; Meili, J. E.; MacDowell, D. W. H.; Wright, M. E. The Rearrangement of Allyl Groups in Three-carbon Systems. VII. Diethyl α-Allyl-2-naphthalenemalonate. *J. Am. Chem. Soc.* **1956**, *78*, 2551–2556.

(4) Tomiczek, B. M.; Grenning, A. J. Aromatic Cope Rearrangements. *Org. Biomol. Chem.* **2021**, *19*, 2385–2398.

(5) Marvell, E. N.; Almond, S. W. The Aromatic Cope Rearrangement: Activation Parameters. *Tetrahedron Lett.* **1979**, 2777–2778.

(6) Woodward, R. B.; Hoffmann, R. Conservation of Orbital Symmetry. *Angew. Chem., Int. Ed.* **1969**, *8*, 781–853.

(7) (a) Maas, G.; Regitz, M. Carbo-Claisen Rearrangement of 8-endo-Phenylbicyclo[5.1.0]octa-2,4-dienes. *Angew. Chem. Int. Ed.*, **1977**, *16*, 711–712. (b) Maas, G. Thermal Rearrangements of 1-Aryl-2-vinylcyclopropanes. *Chem. Ber.* **1979**, *112*, 3241–3272. (c) Maas, G.; Hummel, C. The Heteroaromatic Cope Rearrangement of 1-Pyridyl-, 1-Furyl-, and 1-Thienyl-2-vinylcyclopropanes. *Chem. Ber.* **1980**, *113*, 3679–3696.

(8) (a) De, S.; Tomiczek, B. M.; Yang, Y.; Ko, K.; Ghiviriga, I.; Roitberg, A.; Grenning, A. J. Diastereoselective Indole-Dearomative Cope Rearrangements by Compounding Minor Driving Forces. *Org. Lett.* **2022**, *24*, 3726–3730. (b) Thandavamurthy, K.; Sharma, D.; Porwal, S. K.; Ray, D.; Viswanathan, R. Regioselective Cope Rearrangement and Prenyl Transfers on Indole Scaffold Mimicking Fungal and Bacterial Dimethylallyltryptophan Synthases. *J. Org. Chem.* **2014**, *79*, 10049–10067.

(9) (a) Babinski, D. J.; Bao, X.; El Arba, M.; Chen, B.; Hrovat, D. A.; Borden, W. T.; Frantz, D. E. Synchronized Aromaticity as an Enthalpic Driving Force for the Aromatic Cope Rearrangement. *J. Am. Chem. Soc.* **2012**, *134*, 16139–16142. (b) Abe, T.; Kosaka, Y.; Asano, M.; Harasawa, N.; Mishina, A.; Nagasue, M.; Sugimoto, Y.; Katakawa, K.; Sueki, S.; Anada, M.; Yamada, K. Direct C4-Benzylation of Indoles via Tandem Benzyl Claisen/Cope Rearrangements. *Org. Lett.* **2019**, *21*, 826–829.

(10) Sura, T. P.; MacDowell, D. W. H. Cope Rearrangements in the Benzo[b]thiophene Series. *J. Org. Chem.* **1993**, *58*, 4360–4369.

(11) Abnormal Cope product refers to reactions involving [3,3] sigmatropic rearrangement following by another process than the rearomatisation by [1,3]H shift, see: MacDowell, D. W. H.; Purpura, J. M. Cope Rearrangements in the Thiophene Series. *J. Org. Chem.* **1986**, *51*, 183–188.

(12) (a) Bos, M.; Riguet, E. Iridium-Catalysed Asymmetric Allylic Alkylation of Benzofuran γ-Lactones Followed by Heteroaromatic Cope Rearrangement: Study of an Unusual Reaction Sequence. *Chem. Commun.* **2017**, *53*, 4997–5000. (b) Mando, M.; Grellepois, F.; Blanc, A.; Hénon, E.; Riguet, E. Toward Efficient and Stereoselective Aromatic and Dearomative Cope Rearrangements: Experimental and Theoretical Investigations of α-Ally-α'-Aromatic γ-Lactone Derivatives. *Chem. Eur. J.* **2024**, *30*, e202304138.

(13) (a) Siebert, M. R.; Tantillo, D. J. Transition-State Complexation in Palladium-Promoted [3,3] Sigmatropic Shifts. *J. Am. Chem. Soc.* **2007**, *129*, 8686–8687. (b) Gutierrez, O.; Hendrick, C. E.; Kozlowski, M. C. Divergent Reactivity in Pd-Catalyzed [3,3]-Sigmatropic Rearrangement of Allyloxy- and Propargyloxyindoles Revealed by Computation and Experiment. *Org. Lett.*, **2018**, 20, 6539–6543.

(14) Felix, R. J.; Weber, D.; Gutierrez, O.; Tantillo, D. J.; Gagne, M. R. A Gold-Catalysed Enantioselective Cope Rearrangement of Achiral 1,5-Dienes. *Nat. Chem.* **2012,** *4*, 405–409.

(15) Hashmi, A. S. K.; Hutchings, G. J. Gold Catalysis, *Angew. Chem., Int. Ed.* **2006**, *45*, 7896–7936. (b) Gorin, D. J.; Toste, F. D. Relativistic Effects in Homogeneous Gold Catalysis. *Nature*, **2007**, *446*, 395–403. (c) Hashmi, A. S. K. Introduction: Gold Chemistry. *Chem. Rev.* **2021**, *121*, 8309–8310.

(16) Vidhani, D. V.; Krafft, M. E.; Alabugin, I. V. Gold(I)-Catalyzed Allenyl Cope Rearrangement: Evolution from Asynchronicity to Trappable Intermediates Assisted by Stereoelectronic Switching. *J. Am. Chem. Soc.* **2016**, *138*, 2769–2779.

(17) (a) Lefebvre, C.; Rubez, G.; Khartabil, H.; Boisson, J.-C.; Contreras-García, J.; Hénon, E. Accurately Extracting the Signature of Intermolecular Interactions Present in the NCI Plot of the Reduced Density Gradient versus Electron Density. *Physical Chemistry Chemical Physics*. **2017**, *19*, 17928–17936. (b) Lefebvre, C.; Khartabil, H.; Boisson, J.; Contreras-García, J.; Piquemal, J.; Hénon, E. The Independent Gradient Model: A New Approach for Probing Strong and Weak Interactions in Molecules from Wave Function Calculations. *ChemPhysChem* **2018**, *19*, 724–735. (c) Klein, J.; Khartabil, H.; Boisson, J.-C.; Contreras-Garcia, J.; Piquemal, J.-P.; Hénon, E. A New Way for Probing Bond Strength. *J. Phys. Chem. A* **2020**, 124, 1850–1860.

(18) Silvi, B., Savin, A. Classification of Chemical Bonds Based on Topological Analysis of Electron Localization Functions. *Nature* **1994**, *371*, 683–686.

(19) Mando, M.; Fares, M.; Kowandy, C.; Grellepois, F.; Riguet, E. Organocatalyzed Asymmetric Allylic Alkylation Enables Synthesis of Chiral γ-Lactones Bearing Vicinal Tertiary and Quaternary Stereocenters. *Org. Lett.* **2022**, *24*, 5351−5355. (b) Mando, M.; Grellepois, F.; Riguet, E. Organocatalytic Enantioselective Allylic Alkylation of α-Aryl γ-Lactones: an Approach to Densely Functionalized Quaternary Stereocentres. *Chem. Commun.* **2020**, *56*, 6640−6643.

(20) (a) Ranieri, B.; Escofeta, I.; M. Echavarren, A. M. Anatomy of Gold Catalysts: Facts and Myths. *Org. Biomol. Chem.* **2015**, *13*, 7103−7118. (b) Collado, A.; David J. Nelson, D. J.; Nolan, S. P. Optimizing Catalyst and Reaction Conditions in Gold(I) Catalysis−Ligand and Development. *Chem. Rev.* **2021**, *121*, 8559−8612.

(21) (a) Tzouras, N. V.; Gobbo, A.; Pozsoni, N. B.; Chalkidis, S. G.; Bhandary, S.; Van Hecke, K.; Vougioukalakis, G. C.; Nolan, S. P. Hydrogen Bonding-Enabled Gold Catalysis: Ligand Effects in Gold-Catalyzed Cycloisomerizations in Hexafluoroisopropanol (HFIP). *Chem. Commun.* **2022**, *58*, 8516−8519. (b) Tzouras, N. V.; Zorba, L. P.; Kaplanai, E.; Tsoureas, N.; Nelson, D. J.; Nolan, S. P.; Vougioukalakis, G. C. Hexafluoroisopropanol (HFIP) as a Multifunctional Agent in Gold-Catalyzed Cycloisomerizations and Sequential Transformations. *ACS Catalysis* **2023**, *13*, 8845−8860.

(22) (a) Lu, Z.; Han, O.; Okoromoba, O. E.; Shimizu, N.; Amii, H; Tormena, C. F.; Hammond, G. B.; Xu, B. Predicting Counterion Effects Using a Gold Affinity Index and a Hydrogen Bonding Basicity Index. *Org. Lett.* **2017**, *19*, 5848−5851. (b) Lu, Z.; Li, T.; Mudshinge, S. R.; Xu, B.; Hammond, G. B. Optimization of Catalysts and Conditions in Gold(I) Catalysis-Counterion and Additive Effects. *Chem. Rev.* **2021**, *121*, 8452−8477. (c) Schießl, J.; Schulmeister, J.; Doppiu, A.; Wörner, E.; Rudolph, M.; Karch, R.; Hashmi; A. S. K. An Industrial Perspective on Counter Anions in Gold Catalysis: Underestimated with Respect to "Ligand Effects" *Adv. Synth. Catal.* **2018**, *360*, 2493–2502. (d) Schießl, J.; Schulmeister, J.; Doppiu, A.; Wörner, E.; Rudolph, M.; Karch, R.; Hashmi; A. S. K. An Industrial Perspective on Counter Anions in Gold Catalysis: On Alternative Counter Anions" *Adv. Synth. Catal.* **2018**, *360*, 3949–3959.

(23) Bogojeski, M.; Vogt-Maranto, L.; Tuckerman, M. E.; Müller, K.-R.; Burke, K. Quantum Chemical Accuracy from Density Functional Approximations via Machine Learning. *Nat. Commun.* **2020**, *11*, 5223.

(24) Motiwala, H. F.; Armaly, A. M.; Cacioppo, J. G.; Coombs, T. C.; Koehn, K. R. K.; Norwood, V. M.; Aubé, J. HFIP in Organic Synthesis. *Chem. Rev.* **2022**, 122, 12544−12747.

(25) (a) An, J.; Parodi, A.; Monari, M.; Reis, M. C.; Lopez, C. S.; Bandini, M. Gold-Catalyzed Dearomatization of 2-Naphthols with Alkynes. *Chem. Eur. J.*, **2017**, 23, 17473−17477. (b) Peruzzi, M. T.; Lee, S. J.; Gagné, M. R. Gold(I) Catalyzed Dearomative Claisen Rearrangement of Allyl, Allenyl Methyl, and Propargyl Aryl Ethers. *Org. Lett.*, **2017**, 19, 6256–6259. (c) Weyrauch, J. P.; Hashmi, A. S. K.; Schuster, A.; Hengst, T.; Schetter, S.; Littmann, A.; Rudolph, M.; Hamzic, M.; Visus, J.; Rominger, F.; Frey, W.; Bats J. W. Cyclization of Propargylic Amides: Mild Access to Oxazole Derivatives. *Chem. Eur. J.* **2010**, *16*, 956–963. (d) Hashmi, A. S. K.; Rudolph, M.; Schymura, S.; Visus, J.; Frey, W. Gold Catalysis: Alkylideneoxazolines and -oxazoles from Intramolecular Hydroamination of an Alkyne by a Trichloroacetimidate. *Eur. J. Org. Chem.* **2006**, 4905–4909. (e) Hashmi, A. S. K.; Weyrauch, J. P.; Frey, W.; Bats; J. W. Gold Catalysis: Mild Conditions for the Synthesis of Oxazoles from N-Propargylcarboxamides and Mechanistic Aspects. *Org. Lett.* **2004**, *6*, 4391–4394.

(26) Vidhani, D. V.; Alabugin, I. V. Controlled Evolution of the Cope Rearrangement: Transition from Concerted to Interrupted and Aborted Pericyclic Reactions Regulated by a Switch Built from an Intramolecular Frustrated Lewis Pair. *J. Org. Chem.* **2019**, *84*, 14844−14853.

(27) Chintawar, C. C.; Yadav, A. K.; Kumar, A.; Sancheti, S. P.; Patil, N. T. Divergent Gold Catalysis: Unlocking Molecular Diversity through Catalyst Control. *Chem. Rev.* **2021**, *121*, 8478−8558.

(28) For key role of non-covalent interactions in gold catalysis, see: (a) Liu, D.-Y.; Han, J.; Liu, K.; Cheng, Y.; Tan, H.; Yang, X.; Li, W.; Jin Xie, J. Dinuclear Gold-Catalyzed *para*-Selective C−H Arylation of Undirected Arenes by Noncovalent Interactions. *Angew. Chem. Int. Ed.* **2023**, *62*, e202313122. (b) Jo, T.; Taschinski, S.; Leach, I. F.; Bauer, C.; Hashmi, A. S. K.; Klein, J. E. M. N. On the Role of Noncovalent Ligand-Substrate Interactions in Au(I) Catalysis: An Experimental and Computational Study of Protodeauration *ACS. Catal.* **2022**, *12*, 13158−13163.

(29) Adamo, C.; Barone, V. Toward Reliable Density Functional Methods without Adjustable Parameters: The PBE0 Model. *J. Chem. Phys.* **1999**, *110*, 6158−6170.

(30) Andrae, D.; Häussermann, U.; Dolg, M.; Stoll, H.; Preuss, H. Energy-Adjusted ab Initio Pseudopotentials for the Second and Third Row Transition Elements. *Theor. Chim. Acta* **1990**, *77*, 123–141.

(31) Gaussian 16, Revision C.01, Frisch, M. J.; Trucks, G. W.; Schlegel, H. B.; Scuseria, G. E.; Robb, M. A.; Cheeseman, J. R.; Scalmani, G.; Barone, V.; Petersson, G. A.; Nakatsuji, H.; Li, X.; Caricato, M.; Marenich, A. V.; Bloino, J.; Janesko, B. G.; Gomperts, R.; Mennucci, B.; Hratchian, H. P.; Ortiz, J. V.; Izmaylov, A. F.; Sonnenberg, J. L.; Williams-Young, D.; Ding, F.; Lipparini, F.; Egidi, F.; Goings, J.; Peng, B.; Petrone, A.; Henderson, T.; Ranasinghe, D.; Zakrzewski, V. G.; Gao, J.; Rega, N.; Zheng, G.; Liang, W.; Hada, M.; Ehara, M.; Toyota, K.; Fukuda, R.; Hasegawa, J.; Ishida, M.; Nakajima, T.; Honda, Y.; Kitao, O.; Nakai, H.; Vreven, T.; Throssell, K.; Montgomery, J. A., Jr.; Peralta, J. E.; Ogliaro, F.; Bearpark, M. J.; Heyd, J. J.; Brothers, E. N.; Kudin, K. N.; Staroverov, V. N.; Keith, T. A.; Kobayashi, R.; Normand, J.; Raghavachari, K.; Rendell, A. P.; Burant, J. C.; Iyengar, S. S.; Tomasi, J.; Cossi, M.; Millam, J. M.; Klene, M.; Adamo, C.; Cammi, R.; Ochterski, J. W.; Martin, R. L.; Morokuma, K.; Farkas, O.; Foresman, J. B.; Fox, D. J. Gaussian, Inc., Wallingford CT, **2016**.

(32) Bühl, M.; Reimann, C.; Pantazis, D. A.; Bredow, T.; Neese, F. Geometries of Third-Row Transition-Metal Complexes from Density-Functional Theory. *J. Chem. Theory. Comput.* **2008**, *4*, 1449–1459.

(33) Wang, Y.; Cai, P.-J.; Yu, Z.-X. Mechanistic Study on Gold-Catalyzed Cycloisomerization of Dienediynes Involving Aliphatic C–H Functionalization and Inspiration for Developing a New Strategy to Access Polycarbocycles. *J. Am. Chem. Soc.* **2020**, *142*, 2777–2786.

(34) Tomasi, J.; Mennucci, B.; Cammi, R. Quantum Mechanical Continuum Solvation Models. *Chem. Rev.* **2005**, *105*, 2999–3094.

(35) Canneaux, S.; Bohr, F.; Henon, E. KiSThelP: A Program to Predict Thermodynamic Properties and Rate Constants from Quantum Chemistry Results. *J. Comput. Chem.* **2014**, *35*, 82–93.

(36) Humphrey, W.; Dalke, A.; Schulten, K. VMD - Visual Molecular Dynamics. *J. Molec. Graphics* **1996**, *14*, 33–38.

(37) (a) Kozlowski, D.; Pilmé, J. New Insights in Quantum Chemical Topology Studies Using Numerical Grid-based Analyses. *J. Comput. Chem.* **2011**, *32*, 3207–3217. (b) Chevreau, H.; Pilmé, J. Promising insights in parallel grid-based algorithms for quantum chemical topology. *J. Comput. Chem.* **2023**, *14*, 1505–1516.

(38) Program Tenua, Wachsstock, D. http://cdn.bililite.com/pages/tenua/Tenua-manual.html

TOC

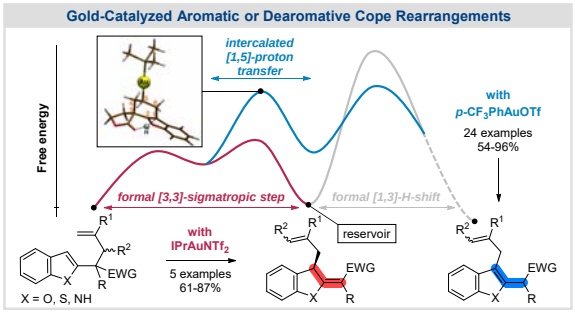
Gold-Catalyzed Aromatic or Dearomative Cope Rearrangements
Free energy
intercalated
[1,5]-proton
transfer
with
p-CF3PhAuOTf
24 examples
54-96%
formal [3,3]-sigmatropic step
formal [1,3]-H-shift
reservoir
with
IPrAuNTf2
5 examples
61-87%
X = O, S, NH
EWG